

Article

# Spatiotemporal Characteristics of Extreme Precipitation Regimes in the Eastern Inland River Basin of Inner Mongolian Plateau, China

Wei Li <sup>1,†</sup>, Limin Duan <sup>1,†</sup>, Yanyun Luo <sup>1</sup>, Tingxi Liu <sup>1,\*</sup> and Buren Scharaw <sup>2</sup>

<sup>1</sup> College of Water Conservancy and Civil Engineering/Inner Mongolia Water Resource Protection and Utilization Key Laboratory, Inner Mongolia Agricultural University, Hohhot 010018, China; liweixl0012@163.com (W.L.); duanlimin820116@163.com (L.D.); luo\_yanyun@163.com (Y.L.)

<sup>2</sup> Institute for Applied Systems Technologies, Fraunhofer IOSB-AST, 98693 Ilmenau, Germany; buren.scharaw@iosb-ast.fraunhofer.de

\* Correspondence: txliu@imau.edu.cn; Tel./Fax: +86-471-430-9386

† These authors contributed equally to this work.

Received: 22 November 2017; Accepted: 1 January 2018; Published: 3 January 2018

**Abstract:** In this work, we use the gridded precipitation dataset (with a resolution of  $0.5^\circ \times 0.5^\circ$ ) of the eastern part of inland river basin of Inner Mongolian Plateau from 1961–2015 as the basis and adopt the methods of climatic diagnosis (e.g., the Modified Mann-Kendall method, principal component analysis, and correlation analysis) to analyze the spatial and temporal variations of six extreme precipitation indices. Furthermore, we analyzed the relationship between El Niño–Southern Oscillation (ENSO) events and the observed extreme precipitation. The results indicated that the gridded dataset can be used to describe the precipitation distribution in our study area. In recent 55 years, the inter-annual variation trends of extreme precipitation indices are generally dominated by declination except for the maximum precipitation over five days (RX5DAY) and the heavy precipitation (R95P), in particular, the decreasing regions of consecutive dry days (CDD) accounts for 91% of the entire basin, 17.28% of which is showing the significant downward trend. Contrary to CDD, the spatial distribution of the other five indices is gradually decreasing from northeast to southwest, and the precipitation intensity (SDII) ranges from 3.8–5.3 mm·d<sup>-1</sup>, with relatively small spatial differences. To some extent, CDD and R95P can be used to characterize the extreme precipitation regimes. Moreover, the number of days with heavy precipitation (RR10), SDII, and R95P are more susceptible to the ENSO events. In addition, the moderate El Niño event may increase the probability of CDD, while the La Niña events may increase the risk of the heavy rainfall regime in the study area.

**Keywords:** inland river basin; extreme precipitation; spatiotemporal variation; Modified Mann-Kendall; ENSO events

## 1. Introduction

Against the background of global warming, the precipitation in some area are generally exhibiting the extreme trend, the intensity and frequency are continuously increasing [1–4]. In recent decades, the disasters that are caused by the frequency occurrence of the precipitation extremes in different countries were more and more serious [5–8]. At the same time, previous studies showed that the climate anomaly have some correlation with El Niño–Southern Oscillation (ENSO) event [9,10], which make the research of extreme climate phenomenon more complicated. In order to regulate the study of extreme climate change characteristics, the World Meteorological Organization (WMO) proposed 27 extreme climate indices (16 extreme temperature indices and 11 extreme precipitation indices) from 1998 to 2001 [11]. Based on these indices, the studies on extreme precipitation events in different regions have also become the focus of global hydrological and meteorological experts [12–14].

The precipitation of China is affected by terrain and multiple climate types, the patterns are particularly complicated. In recent years, the scholars who explored the extreme precipitation events in different regions have scored a lot of remarkable achievements. Some of them used the long sequence precipitation data observed by the national meteorological stations to analyze the extreme precipitation characteristics in the northwest of China, and they found that the persistent drought index in this area shows a decreasing trend, while the other indices, such as precipitation intensity and continuous precipitation days, are on the rise [15–17]. Because of the limited number and the uneven spatial distribution of stations, where the data from can't meet the needs of precision, some other scholars applied the gridded precipitation dataset to solve the problem [18–21], from whose results, we know that the gridded precipitation dataset can also be used to describe the characteristics of precipitation distribution ideally in somewhere, thus the application of gridded precipitation dataset breaks new ground for the studying of extreme precipitation events.

As we know, the extreme hydrological events are closely related to ENSO event; therefore, some studies were investigated to reveal the relationship between them. From the results of their research on the southern watershed in China, we learn that Eastern Pacific Warming induces the heavy precipitation events in summer, while Central Pacific Warming causes the reduction of annual precipitation [9,22,23]. In addition, some other studies also proposed that the extreme precipitation phenomenon in northwest of China is subject to the relatively serious influence of ENSO event [24,25].

As the ecological barrier in the north of China, Inner Mongolia was also affected by the occurrence of precipitation extremes in recent decades, and the most sensitive region is the inland river basin located in the agricultural and pasturing interlaced zone of Inner Mongolian Plateau, where many basins are suffering from the disasters of drought and flood, which exacerbated the deterioration of eco-environment. Although there were some studies on precipitation extremes before, most of them were limited to use the precipitation data from national meteorological stations [26–29], and the accuracy of the results must be affected by the inadequate numbers of stations, in addition, few of them took the ENSO event into consideration. Therefore, we attempt to analyze the spatiotemporal distributions of extreme precipitation regimes characterized by six extreme indices on the basis of the gridded precipitation dataset, further explore the relationship between extreme precipitation event and ENSO event to provide a reference for the management of water resources, flood prevention, and drought mitigation of the grassland in the basin.

## 2. Materials and Methods

### 2.1. Study Area

The  $2.1 \times 10^5$  km<sup>2</sup> study area is located in the eastern part of inland river basin of Inner Mongolian Plateau (111°10'–119°40' E, 41°30'–46°50' N), of which the area of grassland accounts for 95% of the total area. The elevation varies from 620 to 1998 m, and receives an annual average precipitation of 136 to 400 mm, of which the rain falls between June and September and the snow between November and February. The annual potential evapotranspiration of the watershed is 1600 mm or higher, which is much greater than the annual average precipitation, so, the study area belongs to the arid or semi-arid continental monsoon climate.

There are many inland rivers in the basin, such as the Wulagai River, Balageer River, and Xilin River, and so on (Figure 1). The local residents suffered heavy losses that were caused by several extreme precipitation events since the new century. Particularly, the basin suffered a severe drought from 2000 to 2001, when the precipitation and the soil moisture content all fall to a record low, resulting in the reduction of crop yield and the death of a large number of livestock. Meanwhile, in early August 2000, the regional torrential rains initiated the flood, which led to a direct economic loss for about 400 thousand Yuan. Similarly, in June 2008, the flood occurred in the south of the basin forced hundreds of residents to be got trapped. In recent years, the situation regarding drying-up of rivers and degradation of grassland is getting worse, caused by the climate change and human activities.

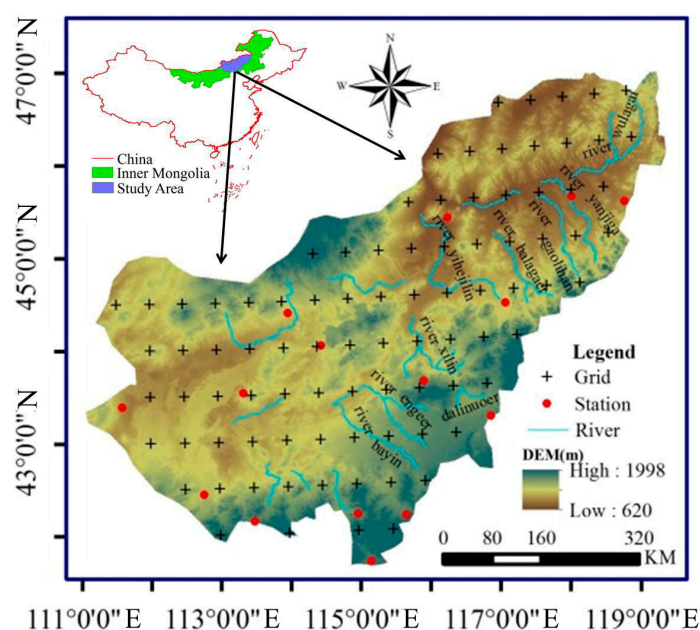


**Figure 1.** Distribution of inland rivers, weather stations, and  $0.5^{\circ} \times 0.5^{\circ}$  grid points.

## 2.2. Data

The gridded daily precipitation dataset (with a resolution of  $0.5^{\circ} \times 0.5^{\circ}$ ) from 1961–2015 came from the National Meteorological Information Center (NMIC) of the China Meteorological Administration (CMA), who interpolated it by the method of Thin Plate Smoothing Splines (TPS) in ANUSPLIN which is a software package published by Australian National University to eliminate the influence of elevation based on the observed daily precipitation over 2400 national meteorological stations across China, and the root-mean-square error (RMSE) of this dataset ranges between 0.2 and 0.8 mm at a monthly scale [21,30–32]. Besides, we also use the measured daily precipitation data with the same time series from 15 meteorological stations in our study area (Table 1) to validate whether the gridded data is suitable for the study area. Both of the two datasets are provided by the NMIC (<http://cdc.nmic.cn>).

**Table 1.** List of the selected meteorological stations in study area.

WMO Number	Station Name	Longitude ( $^{\circ}$ E)	Latitude ( $^{\circ}$ N)	Annual Average Precipitation (mm)
50915	Dongwuqi	116.58	45.31	237.53
53068	Erlianhaote	111.58	43.39	125.75
53192	Abagaqi	114.57	44.01	230.20
53195	Suzuoqi	113.38	43.52	173.47
54012	Xiwuqi	117.36	44.35	314.92
54102	Xilinhaote	116.07	43.57	264.53
53083	Narenbaolige	114.09	44.37	210.13
53276	Zhurihe	112.774	42.44	197.60
50913	Wulagai	118.5	45.43	320.91
50924	Huolinguole	119.3	45.32	345.73
53289	Xianghuangqi	113.5	42.14	270.65
54117	Keshenketengqi	117.02	43.15	391.74
54204	Zhengxiangbaiqi	115	42.18	351.22
54205	Zhenglanqi	115.7	42.14	359.61
54305	Taipusiqi	115.16	41.66	383.47

The data for ENSO event like Sea Surface Temperature Anomalies (SSTA) of Niño 3.4 ( $5^{\circ}$  N– $5^{\circ}$  S,  $170^{\circ}$ – $120^{\circ}$  W) and Southern Oscillation Index (SOI) with the time series from 1961 to 2015 were

obtained from the Earth System Research Laboratory (ESRL) of National Oceanic and Atmospheric Administration (NOAA) (<http://www.esrl.noaa.gov>). In this study, the El Niño events were defined when the values of SSTA are greater than  $0.5^{\circ}$  for a minimum of six consecutive overlapping months. Oppositely, if the values of SSTA are smaller than  $-0.5^{\circ}$  and also can last for more than six months, which would be defined as a La Niña event. Furthermore, the selected El Niño (La Niña) events could be divided into two categories: strong El Niño (La Niña) events have a Niño3.4 index  $>1.0$  ( $<-1.0$ ), and moderate El Niño (La Niña) events with a Niño3.4 index  $>0.5$  and  $\leq 1.0$  ( $<-0.5$  and  $\geq -1.0$ ) [33–35]. According to the criteria, 15 El Niño events and 17 La Niña events were picked out during 1961 to 2015, of which a total of six moderate El Niño, nine strong El Niño, six moderate La Niña, and 11 strong La Niña years were showed in Table 2.

**Table 2.** The selected El Niño and La Niña years and their categories.

Events	Category	Years										
		1965	1972	1982	1983	1987	1992	1997	2009	2015		
El Niño	Strong	1965	1972	1982	1983	1987	1992	1997	2009	2015		
	Moderate	1963	1969	1976	1994	2002	2004					
La Niña	Strong	1973	1974	1975	1988	1989	1998	1999	2000	2007	2008	2010
	Moderate	1964	1970	1971	1985	1995	2011					

In addition, the extreme indices were calculated based on the checked daily precipitation dataset by the RClimDex software (<http://etccdi.pacificclimate.org/software.shtml>), which was developed and maintained by Xuebin Zhang and Feng Yang at the Climate Research Branch, Meteorological Service of Canada [36,37]. We selected six extreme precipitation indices that are widely used [38–41] and are consistent with the climatic characteristics of our study area to evaluate the changes of extreme precipitation regimes. The chosen indices are divided into four different categories: (1) duration indices are defined as the periods of excessive dryness or wetness, such as consecutive dry days (CDD) and consecutive wet days (CWD); (2) absolute indices represent maximum or minimum values within a month or year, such as number of days with daily precipitation  $\geq 10$  mm per year (RR10) and maximum precipitation over five consecutive days in each month (RX5DAY); (3) intensity indices, such as the precipitation intensity (SDII), the mean precipitation amount on a rainy day; and (4) threshold indices defined as the precipitation value falls above a fixed threshold, such as the precipitation higher than the threshold of 95% in one year (R95P) (Table 3).

**Table 3.** Definition of the six extreme precipitation indices.

Category	Index	Abbreviation	Definition	Units
Duration indices	Consecutive dry days	CDD	Maximum consecutive number of days with daily precipitation $<1.0$ mm	days
	Consecutive wet days	CWD	Maximum consecutive number of days with daily precipitation $\geq 1$ mm	days
Absolute indices	Number of days with heavy precipitation	RR10	Total number of days every year with daily precipitation $\geq 10$ mm	days
	Maximum precipitation over 5 days	RX5DAY	Maximum precipitation over five consecutive days in each month	mm
Intensity indices	Precipitation intensity	SDII	The ratio between the annual precipitation and the number of days with daily precipitation $\geq 1$ mm	mm·day <sup>-1</sup>
Threshold indices	Heavy precipitation	R95P	The sum of precipitation with daily precipitation higher than the threshold of 95% in one year	mm

### 2.3. Methods

There is little research by using the precipitation gridded dataset in study area before, so, it is necessary to verify whether the gridded dataset is suitable for the precipitation pattern in the study area. Firstly, the Inverse Distance Weighted (IDW) method was applied for the gridded data interpolation,

which assumes that each point has a local influence that diminishes with distance, and the value of point is more affected by the closer points greater than those further away. The spatial correlation of precipitation data accords with this rule, so it is often used in the spatial interpolation of precipitation. Each meteorological station is surrounded by four grid boxes and the data of which is affected by those four grids most, therefore, the nearest four grid boxes around the specific meteorological station are weighted in the study [21]. What should be noted is when the station is located at the boundary of the basin, the grids should be extended outside to meet the interpolation requirements. The interpolated date was computed as:

$$P_{IDW} = \frac{\sum_{i=1}^n \frac{p_i}{d_i}}{\sum_{i=1}^n \frac{1}{d_i}} \tag{1}$$

where  $p_i$  is the precipitation of the neighboring four grid boxes, respectively;  $d_i$  is the distance between the station and the four surrounded grids;  $n = 4$  in this study.

Secondly, comparing the bias and correlation coefficients between the IDW interpolated data and the observed data from stations [21]. The formula of the bias is given as follows:

$$B = \frac{\overline{P_{IDW}} - \overline{P_{Station}}}{\overline{P_{Station}}} \tag{2}$$

where  $\overline{P_{IDW}}$  is the mean value of interpolated data, and  $\overline{P_{Station}}$  is the means of observed data.

The Modified Mann-Kendall (MM-K) nonparametric test was employed to find the trends of the extreme indices and their significance of trends in time series, which are considered to be statistically significant if it is significant at the 0.1 level. The MM-K test is a rank-based nonparametric trend detection method that is less sensitive to outliers than parametric statistics and does not assume any priority in the distribution of the data and allows for the presence of a tendency over a long period of data. Moreover, it has the advantage of taking the effect of autocorrelation into account [26,42,43], which make the results more accurate. The formulas are given as follows:

$$S = \sum_{k=1}^{N-1} \sum_{j=k+1}^N \text{sign}(x_j - x_k) \tag{3}$$

$$\text{sign}(x_j - x_k) = \begin{cases} 1 & \text{if } x_j > x_k \\ 0 & \text{if } x_j = x_k \\ -1 & \text{if } x_j < x_k \end{cases} \quad (k = 1, 2, \dots, N - 1; j = k + 1, k + 2, \dots, N) \tag{4}$$

$$\text{var}(S) = \frac{N(N-1)(2N+5) - \sum_{p=1}^{N_p} [m_p(m_p-1)(2m_p+5)]}{18} \tag{5}$$

$$\frac{N}{N_S^*} = 1 + \frac{2}{N(N-1)(N-2)} \sum_{i=1}^{N-3} [(N-i)(N-i-1)(N-i-2)(\rho_s(i))] \tag{6}$$

$$\text{var}^*(S) = \text{var}(S) \bullet \left(\frac{N}{N_S^*}\right) \tag{7}$$

$$Z^* = \begin{cases} \frac{S-1}{\sqrt{\text{var}^*(S)}} & \text{if } S > 0 \\ 0 & \text{if } S = 0 \\ \frac{S+1}{\sqrt{\text{var}^*(S)}} & \text{if } S < 0 \end{cases} \tag{8}$$

where  $X$  is the long-term data;  $N$  is the length of  $X$ ;  $N_p$  is the number of distinct ties; and,  $m_p$  is the number of tied data points in  $p$ th tie. If  $Z^* > 0$ , the upward trend was detected. In contrast,

if  $Z^* < 0$ , the downward trend was detected, if  $|Z^*| > 1.64$ , indicating that a significant trend exists at  $\alpha = 0.1$  level.

The magnitude of a trend was estimated using Sen’s slope estimator  $\beta$ , defined as the median of all the possible pairs for the whole series of indices [44]. Computed as:

$$\beta = \text{mean} \left( \frac{x_j - x_i}{j - i}, \forall j > i \right) \tag{9}$$

where  $1 < i < j < n$ ,  $X$  is the time series of data;  $n$  is length of the dataset.

In addition, the five-year smoothing average is also used to show the inter-annual variation of indices. The principal component analysis was applied to partition the dataset into clusters with in-cluster similarities and between-cluster dissimilarities [45] and Pearson correlation analysis was used to examine the linear relationship between extreme precipitation indices and ENSO indices. The spatial distribution maps of extreme indices are finished in ArcGIS 10.

### 3. Results

#### 3.1. Precipitation Change Background

As shown in Figure 2A, we observe that the bias between the IDW interpolated data and the observed data at Erlianhaote station is 17.33%, the highest value among the stations. Meanwhile, the absolute value of the remaining station bias are all less than 15%, of which the vast majority are less than 10%, accounting for 73.33% of the total stations, the accuracy can meet the requirement of such research. In addition, there is a very good linear relationship between the station data and the IDW interpolated data ( $R^2 = 0.98$ ), passed the significance test on the level of 0.0001. Furthermore, the slope of this linear fitting equation reaches 1.08, which is in close proximity to 1.00 (Figure 2B). Therefore, the gridded dataset can reflect the spatiotemporal patterns of precipitation distributions in study area.

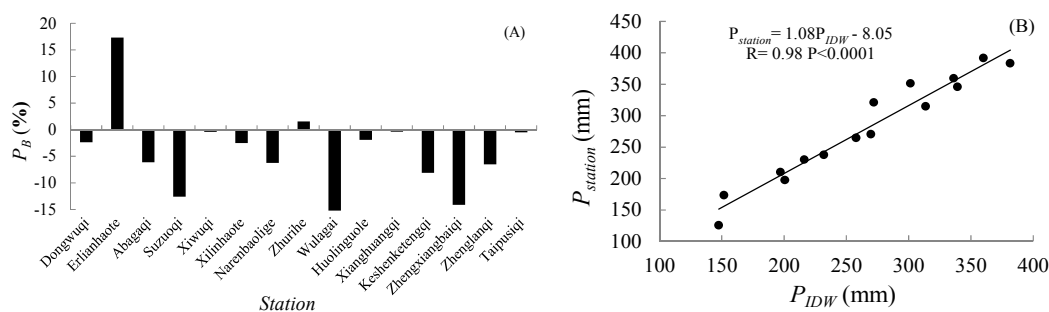


**Figure 2.** Relationship between the observed annual average precipitation and Inverse Distance Weighted (IDW) interpolated precipitation: (A) shows the bias; (B) shows the linear relationship.

The spatial pattern of the annual precipitation in the study area from 1961–2015 exhibits the obvious feature of “high in the northeast and low in the southwest”, and which gradually declines from 376.54 mm in the eastern region to 136.78 mm in the western region. The difference between the annual precipitation in the eastern and western is as high as 240 mm (Figure 3A). Moreover, the precipitation in northeast region exhibits an upward trend with a velocity in excess of 3 mm in a decade ( $\text{mm} \cdot \text{decade}^{-1}$ ), but the region with an increasing trend of precipitation only accounts for 25% of the total area. The remaining 75% is the area where shows an insignificant decreasing trend, mainly being located in the central of the study area (Figure 3B).

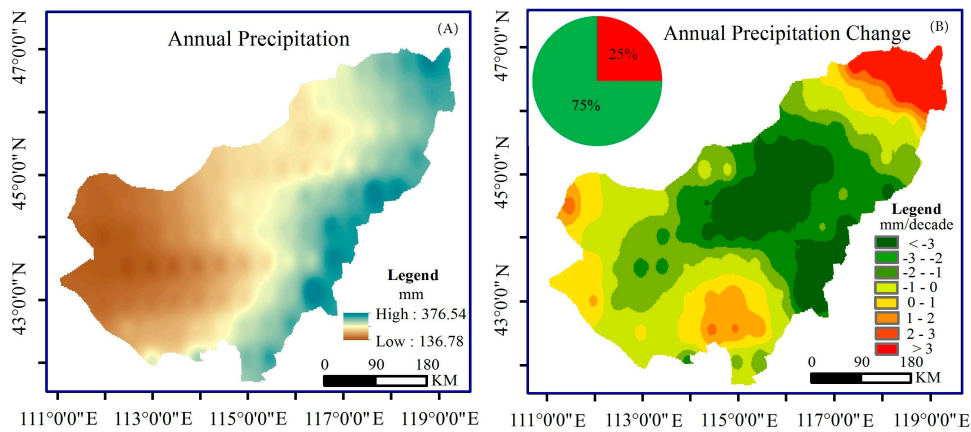


**Figure 3.** Spatiotemporal distribution of the precipitation: (A) shows the spatial distribution of the annual precipitation; (B) shows the spatial distribution of trend magnitude of precipitation at the scale of 10 years. (The red part of the pie chart represents the proportion of the increasing trend, and the green represents the proportion of the decreasing trend).

3.2. Spatiotemporal Variations in Extreme Precipitation Indices

The spatial distributions of the extreme precipitation indices for the eastern part of inland river basin of Inner Mongolian Plateau from 1961–2015 are shown in Figure 4. The consecutive dry days (CDD) are gradually alleviated from southwest to northeast, and the CDD can reach up to 117 days in arid zone of the basin (Figure 4A). Opposite to the spatial variation trend of CDD, the other five extreme indices exhibit the distribution features of “high in the northeast and low in the southwest”. Particularly, the annual average of consecutive wet days (CWD) is 3–8 days, which is generally small and the maximum value appears in the northeast of the study area (Figure 4B). Similarly, the number of days with heavy precipitation (RR10) is range between 3 and 10 days, and heavy precipitation is also mainly occurs in the eastern region (Figure 4C). Regarding the precipitation amount, maximum precipitation over five days (RX5DAY) and heavy precipitation (R95P) decrease gradually from 61.0 mm and 95.0 mm in the northeastern to 28.5 mm and 31.1 mm in the southwestern, respectively (Figure 4D–F). In addition, the average value of R95P is generally higher than RX5DAY. We can find from the SDII diagram that the average precipitation intensity ranges from 3.8 to 5.3 mm·day<sup>-1</sup>, and the spatial difference is not so large (Figure 4E). Except for CDD, the spatial variations of the other five extreme precipitation indices are similar to the variation of the annual precipitation.

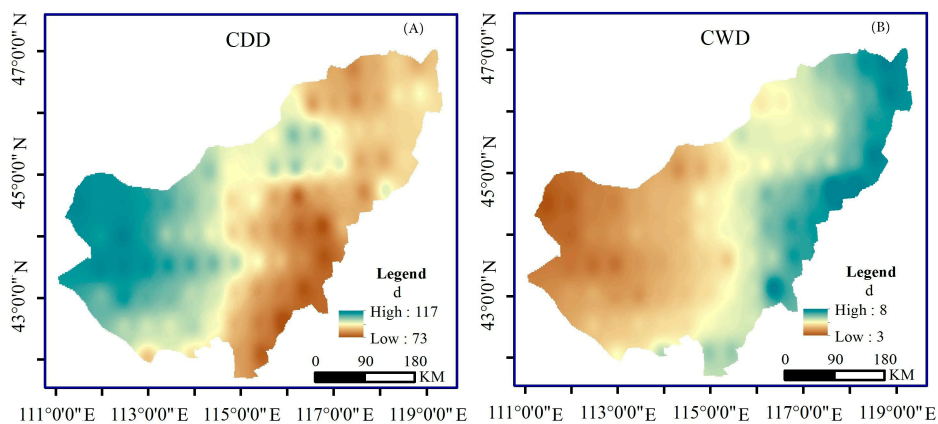


**Figure 4.** Cont.

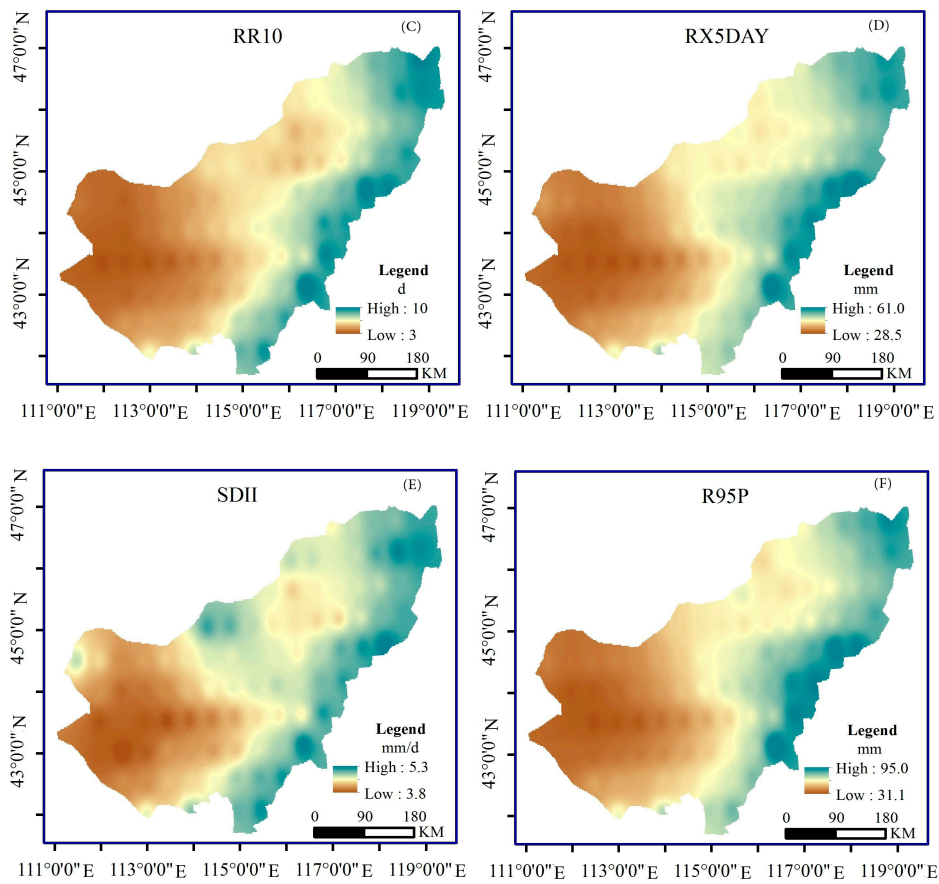


**Figure 4.** Spatial distribution of the average extreme indices: (A) consecutive dry days (CDD); (B) consecutive wet days (CWD); (C) number of days with daily precipitation  $\geq 10$  mm per year (RR10); (D) maximum precipitation over five days (RX5DAY); (E) precipitation intensity (SDII); and, (F) precipitation higher than the threshold of 95% in one year (R95P).

The inter-annual variations of different extreme indices were evaluated by using the average of the values on all the grids. The inter-annual variations were not obvious. In particular, the indices that characterize the heavy precipitation amount (RX5DAY and R95P) exhibit a weak upward trend (Figure 5D–F), and the other indices exhibit a downward trend. In addition, we can also see from the smoothing average curve of five years that SDII was in a stable fluctuation period in the 1970s and increased with a relatively large magnitude from the end of the 1980s to the end of the 1990s. After the end of the 1990s, SDII was again in a stage of stable fluctuation (Figure 5E), which is similar to the variation trend of RR10 (Figure 5C), RX5DAY, and R95P. Both CDD and CWD have always been in a downward stage with fluctuations (Figure 5A,B).

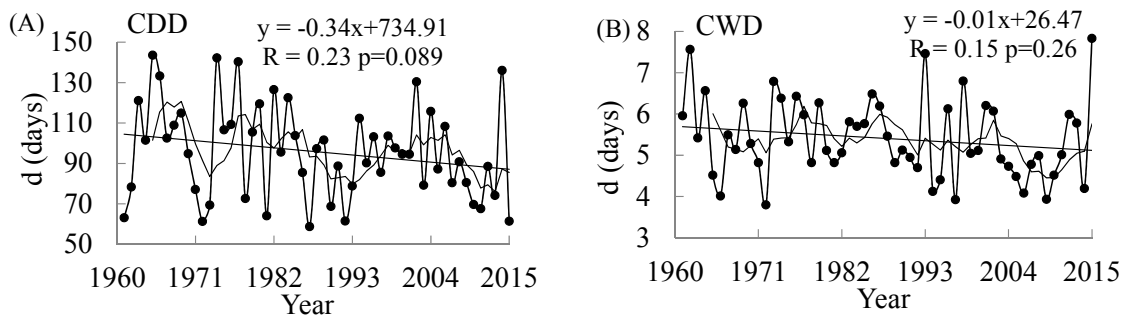


**Figure 5.** Cont.

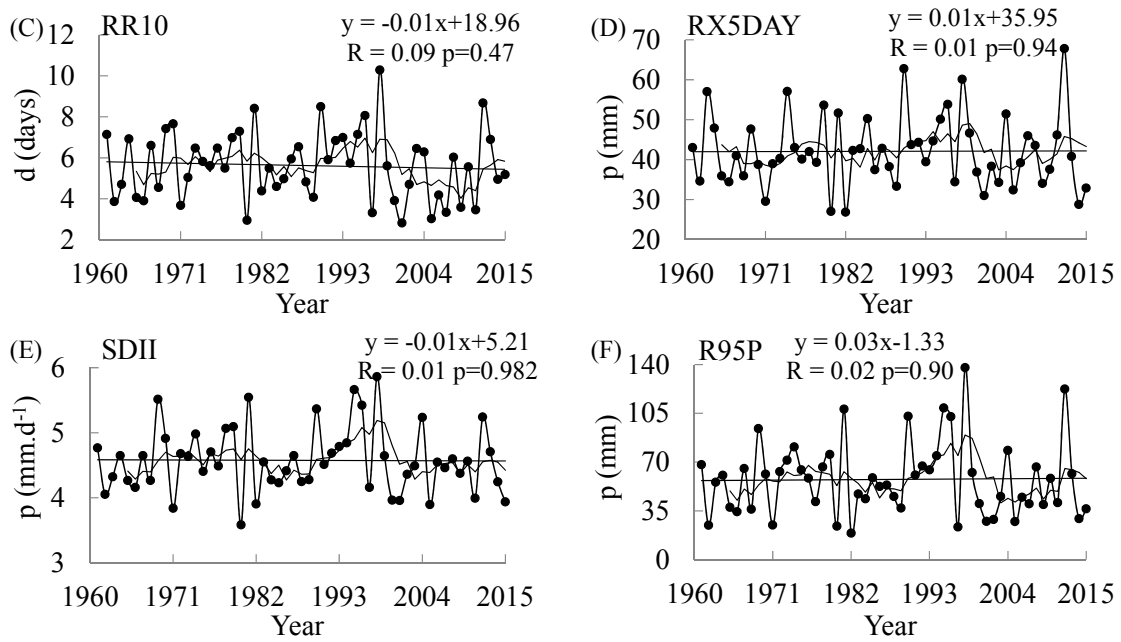


**Figure 5.** Inter-annual change of the extreme precipitation indices: (A) CDD; (B) CWD; (C) RR10; (D) RX5DAY; (E) SDII; and, (F) R95P.

The spatial distributions of the variation magnitude for different extreme indices during the observation period is shown in Figure 6, from which we can see that CDD and CWD are dominated by decline, both of which account for 91% of the study area, the difference is that the former has a significant downward area of 17.28%, while the latter with a significant decreasing trend account for 16% (at a significance level of  $\alpha = 0.1$ ), where mainly located in the south of the study area (Figure 6A,B). We can see from the (Figure 6C) that the variation magnitude of the number of days with heavy precipitation in our study area is relatively small, and does not exceed  $0.3 \text{ mm} \cdot \text{decade}^{-1}$ . Similarly, the variation of RX5DAY is also relatively weak, the region exhibit a downward trend accounts for 29% of the study area (Figure 6D).

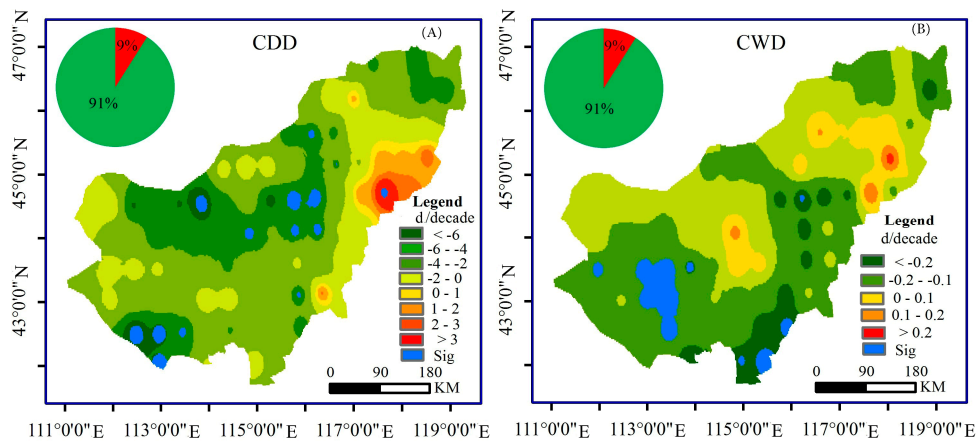


**Figure 6.** Cont.

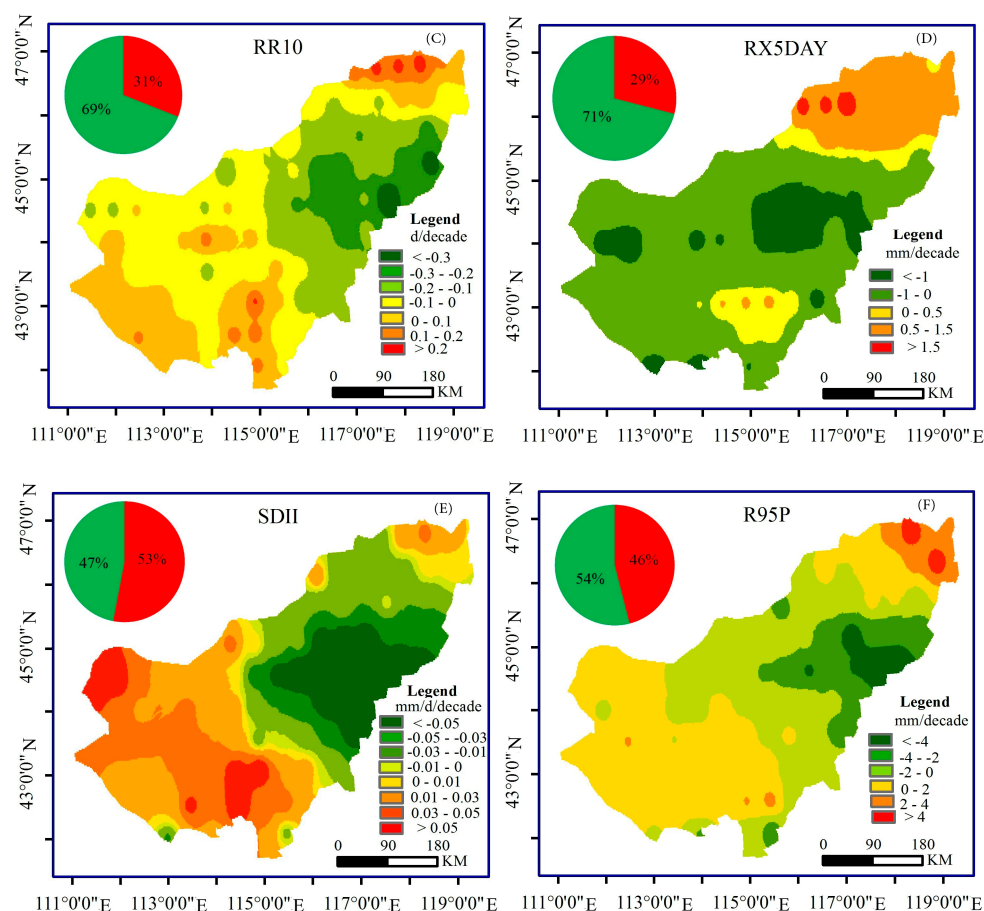


**Figure 6.** Spatial distribution of the variation trend for the extreme precipitation indices: (A) CDD; (B) CWD; (C) RR10; (D) RX5DAY; (E) SDII; and, (F) R95P. (The red part of the pie chart represents the proportion of the increasing trend, and the green represents the proportion of the decreasing trend).

In spite of this, the region of SDII shows an upward trend (53%), the area of which exceed the downward area (47%), and the variation magnitude is extremely small, therefore, the performance of the precipitation intensity exhibit the downward trend (Figure 6E). The spatial distribution of the variation magnitude for R95P is dominated by the decreasing trend, being mainly located in the central of study area, which accounts for 54% of the research area, in addition, the magnitude of this increase in the northeastern area is 2–6  $\text{mm}\cdot\text{decade}^{-1}$ , which is greater than 0–2  $\text{mm}\cdot\text{decade}^{-1}$  in the southwestern area (Figure 6F). None of the other four indices exhibits a significant changing trend expect for CDD and CWD.

### 3.3. Factor Analysis of Extreme Precipitation Indices

After analyzing the annual precipitation and the six extreme indices by principal component analysis, the results show that the first principal component accounts for 61.34% of the total variance, which included almost all of the indices except for CDD and CWD, and the loads of the component indices are all exceed 0.80, particularly, R95P has a maximum load of 0.96, which reflects that R95P has the indicative function for the whole heavy rainfall regime. In addition, the variance contribution rate of the second component is 16.25%, and the loads of CDD and CWD are relatively high, are 0.64 and  $-0.72$ , respectively. Therefore, this kind of extreme event can be defined as the drought regime, which is characterized by CDD (Table 4).

**Table 4.** Factor analysis of extreme precipitation indices.

Component	Annual Precipitation	CDD	CWD	SDII	RR10	RX5DAY	R95P	Percentage/%
1	0.90	−0.21	0.34	0.91	0.94	0.84	0.96	61.34
2	−0.24	0.64	−0.72	0.26	−0.24	0.24	0.19	16.25

Note: KMO: 0.78; Bartlett: 361.12;  $p < 0.001$ .

The Pearson correlation coefficients between annual precipitation and extreme indices are shown in Table 5 to verify the relationships between them. In addition to CDD, the other five extreme indices have positive correlations with the annual precipitation and their correlation coefficients are statistically significant at the 0.01 level. The negative correlation coefficient between CDD and CWD reaches 0.60 (at a significance level of  $\alpha = 0.05$ ), but the correlation between this two extreme indices and the other four indices is relatively poor. When comparing the behavior of the remaining four extreme indices, R95P has the strongest correlations with the other three indices, and all of the correlations coefficients fell in the confidence interval under the 99% confidence level, which further validates the results in Table 4. To some extent, CDD and R95P can characterize the two kinds of extreme precipitation events we defined as the drought event and the heavy rainfall event well, and the two kinds of extreme events form the extreme precipitation events in our study.

**Table 5.** Correlation coefficients of extreme precipitation indices.

Precipitation Regime	Annual Precipitation	CDD	CWD	SDII	RR10	RX5DAY	R95P
Annual Precipitation	1						
CDD	−0.26	1					
CWD	0.48 **	−0.6 *	1				
SDII	0.72 **	−0.13	0.18	1			
RR10	0.89 **	−0.20	0.34 **	0.88 **	1		
RX5DAY	0.59 **	−0.01	0.26 *	0.73 **	0.64 **	1	
R95P	0.77 **	−0.16	0.20	0.92 **	0.86 **	0.82 **	1

Note: \*\* Significant at the 0.01 level; \* Significant at the 0.05 level.

### 3.4. Response of the Extreme Precipitation Indices to ENSO Event

The Pearson correlation coefficients between the six extreme precipitation indices and the two ENSO indices were calculated in Table 6, and there are obvious differences between them. CDD has a negative correlation with SSTA from January to June, and has positive correlation with it from July to December. However, in terms of the correlation with SSTA, the other five indices have almost the opposite features with CDD at monthly scale. Including the positive correlations of RR10 and SDII with SSTA from January to April, which are statistically significant at the 0.05 level, and the negative correlations from June to December. In addition, R95P is also showing a significant negative correlation with SSTA (at a significance level of  $\alpha = 0.1$ ) from September to December. Furthermore, the correlation relationship between each extreme index and SOI is opposite to the relationship of which with SSTA, except in May, respectively. It means that if the extreme index showing a negative (positive) correlation with SSTA, it will appear a positive (negative) correlation with SOI at the same month. Both RR10 and SDII are closely related with SOI as well (at a significance level of  $\alpha = 0.05$ ) from January to April. In general, RR10, SDII, and R95P are particularly sensitive to ENSO in our study area.

**Table 6.** Correlation between extreme precipitation indices and Sea Surface Temperature Anomalies (SSTA) and Southern Oscillation Index (SOI).

Month	CDD		CWD		RR10		RX5DAY		SDII		R95P	
	SSTA	SOI	SSTA	SOI	SSTA	SOI	SSTA	SOI	SSTA	SOI	SSTA	SOI
January	−0.14	0.13	0.18	−0.07	0.32 **	−0.33 **	0.04	−0.11	0.25 **	−0.28 **	0.18	−0.23 **
February	−0.17	0.24 *	0.22	−0.10	0.35 **	−0.33 **	0.08	−0.03	0.29 **	−0.26 **	0.27	−0.13
March	−0.18	0.16	0.20	−0.03	0.35 **	−0.27 **	0.05	−0.01	0.28 **	−0.26 **	0.20	−0.12
April	−0.21	−0.03	0.12	−0.04	0.26 **	−0.28 **	−0.03	−0.08	0.26 **	−0.33 **	0.12	−0.23 *
May	−0.13	0.02	0.03	0.11	0.14	0.19	−0.06	0.21	0.12	0.17	0.03	0.19
June	−0.03	−0.08	−0.17	0.13	−0.08	0.23 **	−0.19	0.12	−0.06	0.23 *	−0.17	0.26 *
July	0.01	−0.17	−0.21	0.03	−0.16	0.19	−0.13	0.12	−0.13	0.17	−0.21	0.28 **
August	0.07	−0.15	−0.17	0.06	−0.14	0.17	−0.09	0.21	−0.10	0.11	−0.17	0.25 *
September	0.12	−0.18	−0.20	0.08	−0.12	0.10	−0.14	0.15	−0.10	0.07	−0.20 *	0.17
October	0.14	−0.11	−0.22	0.14	−0.13	0.04	−0.21	0.09	−0.20	−0.02	−0.22 *	0.09
November	0.12	−0.37 *	−0.22	0.16	−0.12	0.12	−0.23 *	0.11	−0.12	0.08	−0.22 *	0.20
December	0.11	−0.27 *	−0.23 *	0.04	−0.14	0.13	−0.22	0.10	−0.12	0.10	−0.23 *	0.17

Note: \*\* Significant at the 0.05 level; \* Significant at the 0.1 level.

Table 7 shows how the extreme precipitation indices in a specific ENSO period deviate from the normal period in detail. The values were calculated by the average of the indices that correspond with the years of the specific ENSO category. The average consecutive dry days in moderate El Niño years are as many as 117 days, 21 days more than which in normal years, while there are only 87 days in strong El Niño years, moreover, no matter the moderate or strong La Niña events happened, the values of CDD are always decreased. The situation of CDD is similar to that of CWD.

**Table 7.** Average values of extreme precipitation indices in different El Niño–Southern Oscillation (ENSO) years and normal years.

Events	CDD (Days)	CWD (Days)	RR10 (Days)	RX5DAY (mm)	SDII (mm·day <sup>−1</sup> )	R95P (mm)
El Niño-Strong	87.00	5.00	5.00	36.95	4.36	42.99
El Niño-Moderate	117.00	6.00	6.00	46.54	4.83	64.95
Normal	96.00	6.00	6.00	41.61	4.57	57.79
La Niña-Strong	94.00	5.00	6.00	43.87	4.60	64.01
La Niña-Moderate	90.00	5.00	6.00	43.80	4.55	59.20

From different values of RR10 in the five periods, we can find that there is little difference between each other, which indicates that ENSO events have limited influence on RR10 in study area. For RX5DAY, the strong El Niño events reduce the maximum precipitation over five days by 4.66 mm, while the moderate El Niño events increase it by 4.93 mm. Additionally, approximately 2.20 mm is increased by the occurrence of both two categories La Niña events compared to the normal years for RX5DAY. The influence of different ENSO periods on RX5DAY is almost identical with R95P, the only difference is the amplitudes of R95P between ENSO years and normal years are relatively larger than RX5DAY. The maximum value of precipitation intensity appears in moderate El Niño years, and SDII in strong La Niña years is also greater than in normal years. However, during strong El Niño years and moderate La Niña years, the values are both smaller than in normal years.

In summary, the values of extreme precipitation indices in moderate El Niño are usually greater than of which in normal years, but in strong El Niño years, these values are always the smallest. The both two kinds of La Niña events may decrease the values of CDD and CWD, but increase the values of RX5DAY and R95P.

#### 4. Discussion

The limited number and the uneven spatial distribution of meteorological stations in our study area are the main reasons why we apply the gridded precipitation dataset for this study. By comparing the bias and correlation coefficients between IDW interpolated precipitation data and station precipitation data, we found that it was highly similar with each other. Moreover, the interpolated data was calculated by using the spatial interpolation method (IDW) that was based on the gridded dataset, it means that the values of grid boxes around the station are also highly similar

with the station data. Therefore, it is considered that the gridded precipitation dataset can be used to describe the precipitation distribution pattern accurately in our study area.

The eastern part of inland river basin of Inner Mongolian Plateau is located in high attitude inland area, where surrounded by the Daxinganling Mountains and Yinshan Mountains, the warm-wet air is different to penetrate through the territory, thus forming the climatic features of scarce precipitation but intensive evaporation [46,47]. In recent decades, because of the increasing air pressure led by the high-latitude circulation anomaly and the inter-annual decrease of East Asian Monsoon, along with the decrease of water vapor transport to the north, the number of consecutive wet days, and the precipitation intensity are all reducing [17,48], which eventually led to a further decline in precipitation in our study area [26,49]. In that context, the indices represent the extreme precipitation and precipitation days in study area show the distribution characteristics of “high in the northeast and low in the southwest”, and the values of northeast are on the rise, which suggests that flooding is prone to take place in the northeastern part of study area, and that the probability of the disaster is increasing. In addition, the persistent drought is still heavy, especially in the western part of the basin, but the phenomenon were eased up in the past 55 years, which is in agreement with the findings of previous work [50].

The extreme precipitation regimes in our study can be divided into two categories by the factor analysis method, the drought regime, and the heavy rainfall regime, which can be characterized by CDD and R95P, and the two extreme indices have good correlations with other indices belong to a same category of regime, respectively [18]. Furthermore, the extreme indices have good correlations with ENSO indices, of which RR10, SDII, and R95P are more sensitive to ENSO. Specifically, the moderate El Niño event may be the main reason of the drought, while the occurrence of La Niña events may increase the risk of floods, which is similar to the previous study [51]. It is suggested that the ENSO events have a driving effect on the extreme precipitation regimes in the study area. Overall, the study revealed long-term spatiotemporal variability of the extreme precipitation indices, and the response to ENSO event, which can provide a scientific basis for helping to generate water resources management plans. However, there are many other factors, such as human activities and atmospheric circulation, to affect the change of precipitation, therefore, the studies that consider the factors above should be further conducted in detail.

## 5. Conclusions

Based on the gridded precipitation dataset with horizontal resolution of  $0.5^{\circ} \times 0.5^{\circ}$  in the eastern part of inland river basin of Inner Mongolian Plateau from 1961 to 2015, we employed the Sen's slop and the MM-K nonparametric test together with the factor analysis methods to research the spatiotemporal variability of extreme precipitation regimes presented by six extreme indices, meanwhile, the response of extreme precipitation events to ENSO events are discussed. The main conclusions are as follows:

- (1) The gridded precipitation dataset is suitable for the characterization of precipitation distribution in the study area, and the spatial pattern of precipitation is obviously characterized by the “high in northeast and low in southwest” in the study area. Meanwhile, a non-significantly decreasing inter-annual tendency was found during the 55 years, where it is mainly located in the central of the study area.
- (2) The CDD is more severe in the southwest of the watershed. But, beyond this, the spatial distributions of the other five indices and the annual precipitation are the same, whose spatial pattern is gradually decreasing from northeast to southwest. The values of CWD and RR10 in the study area are relatively low, while the spatial difference of SDII is not obvious, between 3.8 and 5.3  $\text{mm}\cdot\text{d}^{-1}$ . In terms of the temporal distributions of the extreme precipitation indices, which mainly showing a decreasing trend except for RX5DAY and R95P, of which 17.28% and 16.00% of the regions show the significant downward trends (at a significance level of  $\alpha = 0.1$ ), which belong to the decreasing area of CDD and CWD during the period of 1961–2015, respectively.

- (3) To some extent, CDD and R95P can be used to characterize the drought regime and the heavy rainfall regime, respectively, and both have strong correlations (at a significance level of  $\alpha = 0.1$ ) with the other indices that belong to the same category of extreme event. The selected two categories of extreme regimes compose the whole extreme precipitation regimes in this study.
- (4) Extreme precipitation indices have good correlations with SSTA and SOI in the study area, but the correlation relationship with the two ENSO indices are almost the opposite. In addition, the correlation relationships of CDD and the other five indices with the ENSO indices is also the opposite. RR10, SDII, and R95P are more susceptible to the ENSO events in the study area. Furthermore, the moderate El Niño event may increase the probability of the consecutive dry days, while the strong El Niño event will decrease the probability of extreme regimes in our study area. Meanwhile, the occurrence of La Niña events may increase the risk of the heavy rainfall regime.

**Acknowledgments:** This work was financially supported by the International S&T Cooperation Program of China (No. 2015DFA00530), the National Natural Science Foundation of China (Nos. 51620105003, 51509131 and 51139002), the Science and Technology Major Project of Inner Mongolia Autonomous Region (No. 206202100), the Inner Mongolia Scientific Research Project of University (No. NJZY064), the Ministry of Education Innovative Research Team (No. IRT\_17R60), the Innovation Team in Priority Areas Accredited by the Ministry of Science and Technology (No. 2015RA4013), the Natural Science Foundation of Inner Mongolia (Nos. 2015BS0514 and 2015MS0566), the program for Young Talents of Science and Technology in Universities of Inner Mongolia Autonomous Region (No. NJYT-18-B11) and the Excellent Young Scientist Foundation of Inner Mongolia Agricultural University of China (Grant No. 2014XYQ-11).

**Author Contributions:** Wei Li and Limin Duan developed the initial and final versions of this manuscript and analyzed the data together. Yanyun Luo, Tingxi Liu and Buren Scharaw contributed their expertise and insights, overseeing all of the analysis and supporting the writing of the final manuscript.

**Conflicts of Interest:** The authors declare no conflict of interest.

## References

1. Utsumi, N.; Seto, S.; Kanae, S.; Utsumi, N.; Maeda, E.E.; Oki, T. Does higher surface temperature intensify extreme precipitation? *Geophys. Res. Lett.* **2011**, *38*, 16708–16712. [[CrossRef](#)]
2. Fu, G.B.; Yu, J.J.; Yu, X.B.; Ouyang, R.L.; Zhang, Y.C.; Wang, P.; Liu, W.B.; Min, L.L. Temporal variation of extreme rainfall events in China, 1961–2009. *J. Hydrol.* **2013**, *487*, 48–59. [[CrossRef](#)]
3. Jones, M.R.; Blenkinsop, S.; Fowler, H.J.; Kilsby, C.G. Objective classification of extreme rainfall regions for the UK and updated estimates of trends in regional extreme rainfall. *Int. J. Climatol.* **2014**, *34*, 751–765. [[CrossRef](#)]
4. Westra, S.; Fowler, H.J.; Evans, J.P.; Alexander, L.V.; Berg, P.; Johnson, F.; Kendon, E.J.; Lenderink, G.; Roberts, N.M. Future changes to the intensity and frequency of short-duration extreme rainfall. *Rev. Geophys.* **2014**, *52*, 522–555. [[CrossRef](#)]
5. Li, Z.; Zheng, F.L.; Liu, W.Z.; Flanagan, D.C. Spatial distribution and temporal trends of extreme temperature and precipitation events on the loess plateau of China during 1961–2007. *Quat. Int.* **2010**, *226*, 92–100. [[CrossRef](#)]
6. Sternberg, T.; Thomas, D.; Middleton, N. Drought dynamics on the Mongolian steppe 1970–2006. *Int. J. Climatol.* **2011**, *31*, 1823–1830. [[CrossRef](#)]
7. Wang, K.; Wang, L.; Wei, Y.M.; Ye, M.S. Beijing storm of July 21, 2012: Observations and reflections. *Nat. Hazards* **2013**, *67*, 969–974. [[CrossRef](#)]
8. Li, Q.F.; Li, P.C.; Li, H.Y.; Yu, M.X. Drought assessment using a multivariate drought index in the Luanhe River basin of Northern China. *Stoch. Environ. Res. Risk Assess.* **2015**, *29*, 1509–1520. [[CrossRef](#)]
9. Zhang, Q.; Li, J.F.; Singh, V.P.; Xu, C.Y.; Deng, J.Y. Influence of ENSO on precipitation in the East River basin, South China. *J. Geophys. Res.* **2013**, *118*, 2207–2219. [[CrossRef](#)]
10. Liu, Z.Y.; Menzel, L.; Dong, C.Y.; Fang, R.H. Temporal dynamics and spatial patterns of drought and the relation to ENSO: A case study in Northwest China. *Int. J. Climatol.* **2016**, *36*, 2886–2898. [[CrossRef](#)]
11. Peterson, T.C.; Folland, C.; Gruza, G.; Hogg, W.; Mokssit, A.; Plummer, N. Report on the Activities of the Working Group on Climate Change Detection and Related Rapporteurs 1998–2001. WMO, Rep. WCDMP-47,

- WMO-TD 1071, Geneva, Switzerland, 143p. Available online: <http://etccdi.pacificclimate.org> (accessed on 15 June 2016).
12. Gelati, E.; Madsen, H.; Rosbjerg, D. Stochastic reservoir optimization using El Niño information: Case study of Daule Peripa, Ecuador. *Hydrol. Res.* **2011**, *42*, 413–431. [[CrossRef](#)]
  13. Parry, S.; Hannaford, J.; Lloyd, H.B.; Prudhomme, C. Multi-year droughts in Europe: Analysis of development and causes. *Hydrol. Res.* **2012**, *43*, 689–706. [[CrossRef](#)]
  14. Skaugen, T.; Stranden, H.B.; Saloranta, T. Trends in snow water equivalent in Norway (1931–2009). *Hydrol. Res.* **2012**, *43*, 489–499. [[CrossRef](#)]
  15. You, Q.L.; Kang, S.K.; Aguilar, E.; Pepin, N.; Flugel, W.A.; Yan, Y.P.; Xu, Y.W.; Zhang, Y.J.; Huang, J. Changes in daily climate extremes in China and their connection to the large scale atmospheric circulation during 1961–2003. *Clim. Dyn.* **2011**, *36*, 2399–2417. [[CrossRef](#)]
  16. Wang, B.L.; Zhang, M.J.; Wei, J.L.; Wang, S.J.; Li, X.F.; Li, S.S.; Zhao, A.F.; Li, X.S.; Fan, J.P. Changes in extreme precipitation over Northeast China, 1960–2011. *Quat. Int.* **2013**, *298*, 177–186. [[CrossRef](#)]
  17. Huang, J.; Sun, S.L.; Xue, Y.L.; Zhang, J.C. Changing characteristics of precipitation during 1960–2012 in Inner Mongolia, northern China. *Meteorol. Atmos. Phys.* **2015**, *127*, 257–271. [[CrossRef](#)]
  18. Wang, S.J.; Zhang, M.J.; Sun, M.P.; Wang, B.L.; Li, X.F. Changes in precipitation extremes in alpine areas of the Chinese Tianshan Mountains, central Asia, 1961–2011. *Quat. Int.* **2013**, *311*, 97–107. [[CrossRef](#)]
  19. You, Q.L.; Zhang, M.J.; Zhang, W.; Pepin, N.; Kang, S.C. Comparison of multiple datasets with gridded precipitation observations over the Tibetan Plateau. *Clim. Dyn.* **2015**, *45*, 791–806. [[CrossRef](#)]
  20. Zhu, X.F.; Zhang, M.J.; Wang, S.J.; Qiang, F.; Zeng, T.; Ren, Z.G.; Dong, L. Comparison of monthly precipitation derived from high-resolution gridded datasets in arid Xinjiang, central Asia. *Quat. Int.* **2015**, *358*, 160–170. [[CrossRef](#)]
  21. Qiang, F.; Zhang, M.J.; Wang, S.J.; Liu, Y.M.; Ren, Z.G.; Zhu, X.F. Estimation of areal precipitation in the Qilian Mountains based on a gridded dataset since 1961. *J. Geogr. Sci.* **2016**, *26*, 59–69. [[CrossRef](#)]
  22. Zhang, Q.; Xu, C.Y.; Jiang, T.; Wu, Y.J. Possible influence of ENSO on annual maximum stream flow of the Yangtze River, China. *J. Hydrol.* **2007**, *333*, 265–274. [[CrossRef](#)]
  23. Wang, Y.; Zhang, Q.; Zhang, S.; Chen, X.H. Spatial and Temporal Characteristics of Precipitation in the Huaihe River Basin and Its Response to ENSO Events. *Sci. Geogr. Sin.* **2016**, *36*, 128–134. [[CrossRef](#)]
  24. Li, S.S.; Yang, S.N.; Liu, X.F. Spatiotemporal variability of extreme precipitation in north and south of the Qinling-Huaihe region and influencing factors during 1960–2013. *Prog. Geogr.* **2015**, *34*, 354–363. [[CrossRef](#)]
  25. Jiang, R.G.; Xie, J.C.; Zhao, Y.; He, H.L.; He, G.H. Spatiotemporal variability of extreme precipitation in Shanxi province under climate change. *Theor. Appl. Climatol.* **2017**, *130*, 831–845. [[CrossRef](#)]
  26. Wang, X.X.; Yang, X.M.; Liu, T.X.; Li, F.L.; Gao, R.Z.; Duan, L.M.; Luo, Y.Y. Trend and extreme occurrence of precipitation in a mid-latitude Eurasian steppe watershed at various time scales. *Hydrol. Processes* **2014**, *28*, 5547–5560. [[CrossRef](#)]
  27. Yan, H.M.; Chen, W.N.; Yang, F.X.; Liu, J.Y.; Hu, Y.F.; Ji, Y.Z. The spatial and temporal analysis of extreme climatic events in Inner Mongolia during the past 50 years. *Geogr. Res.* **2014**, *33*, 13–22. [[CrossRef](#)]
  28. Guo, Q.; Hu, Z.M.; Li, S.G.; Yu, G.R.; Sun, X.M.; Zhang, L.M.; Mu, S.L.; Zhu, X.J.; Wang, Y.F.; Li, Y.N.; et al. Contrasting responses of gross primary productivity to precipitation events in a water-limited and a temperature-limited grassland ecosystem. *Agric. For. Meteorol.* **2015**, *214–215*, 169–177. [[CrossRef](#)]
  29. Guo, Q.; Hu, Z.M.; Zhao, W.; Yu, G.R.; Sun, X.M.; Li, L.H.; Liang, N.S.; Bai, W.M. Responses of gross primary productivity to different sizes of precipitation events in a temperate grassland ecosystem in Inner Mongolia, China. *J. Arid Land* **2016**, *8*, 36–46. [[CrossRef](#)]
  30. Wang, B.L.; Zhang, M.J.; Wei, J.L.; Wang, S.J.; Li, S.S.; Ma, Q.; Li, X.F.; Pan, S.K. Changes in extreme events of temperature and precipitation over Xinjiang, northwest China, during 1960–2009. *Quat. Int.* **2013**, *298*, 141–151. [[CrossRef](#)]
  31. Zhao, Y.F.; Zhu, J.; Xu, Y. Establishment and assessment of the grid precipitation datasets in China for recent 50 years. *J. Meteorol. Sci.* **2014**, *34*, 414–420. [[CrossRef](#)]
  32. Ren, Z.G.; Zhang, M.J.; Wang, S.J.; Qiang, F.; Zhu, X.F.; Dong, L. Changes in daily extreme precipitation events in South China from 1961 to 2011. *J. Geogr. Sci.* **2015**, *25*, 58–68. [[CrossRef](#)]
  33. Ropelewski, C.F.; Jones, P.D. An extension of the Tahiti-Darwin Southern Oscillation Index. *Mon. Weather Rev.* **1987**, *115*, 2161–2165. [[CrossRef](#)]

34. Jia, X.J.; Ge, J.W.; Wang, S. Diverse impacts of ENSO on wintertime rainfall over the Maritime Continent. *Int. J. Climatol.* **2016**, *36*, 3384–3397. [[CrossRef](#)]
35. Llamedo, P.; Hierro, R.; Torre, A.; Alexander, P. ENSO-related moisture and temperature anomalies over South America derived from GPS radio occultation profiles. *Int. J. Climatol.* **2016**, *37*, 268–275. [[CrossRef](#)]
36. Zhang, K.X.; Pan, S.M.; Cao, L.G.; Wang, Y.; Zhao, Y.F.; Zhang, W. Spatial distribution and temporal trends in precipitation extremes over the Hengduan Mountains region, China, from 1961 to 2012. *Quat. Int.* **2014**, *349*, 346–356. [[CrossRef](#)]
37. Gao, Y.; Feng, Q.; Liu, W.B.; Lu, A.G.; Wang, Y.; Yang, J.; Cheng, A.F.; Wang, Y.M.; Su, Y.B.; Liu, L.; et al. Changes of daily climate extremes in Loess Plateau during 1960–2013. *Quat. Int.* **2015**, *371*, 5–21. [[CrossRef](#)]
38. Frich, P.; Alexander, L.V.; Della-Marta, P.; Gleason, B.; Haylock, M.; Tank, A.K.; Peterson, T. Observed coherent changes in climatic extremes during the second half of the twentieth century. *Clim. Res.* **2002**, *19*, 193–212. [[CrossRef](#)]
39. Liu, X.D.; Cheng, Z.G.; Yan, L.B.; Yin, Z.Y. Elevation dependency of recent and future minimum surface air temperature trends in the Tibetan Plateau and its surroundings. *Glob. Planet. Chang.* **2009**, *68*, 164–174. [[CrossRef](#)]
40. Sohrabi, M.M.; Ryu, J.H.; Abatzoglou, J.; Tracy, J. Climate extreme and its linkage to regional drought over Idaho, USA. *Nat. Hazards* **2013**, *65*, 653–681. [[CrossRef](#)]
41. Skansi, M.M.; Brunet, M.; Sigró, J.; Aguilarb, E.; Groeningd, J.A.A.; Oscar, J.; Bentancure, O.J.; Geierf, Y.R.C. Warming and wetting signals emerging from analysis of changes in climate extreme indices over South America. *Glob. Planet. Chang.* **2013**, *100*, 295–307. [[CrossRef](#)]
42. Hamed, K.H.; Rao, R.A. A modified Mann-Kendall trend test for autocorrelated data. *J. Hydrol.* **1998**, *204*, 182–196. [[CrossRef](#)]
43. Yue, S.; Wang, C.Y. The Mann-Kendall Test Modified by Effective Sample Size to Detect Trend in Serially Correlated Hydrological Series. *Water Resour. Manag.* **2004**, *18*, 201–218. [[CrossRef](#)]
44. Sen, P.K. Estimates of the regression coefficient based on Kendall's tau. *J. Am. Stat. Assoc.* **1968**, *39*, 1379–1389. [[CrossRef](#)]
45. Li, Z.X.; He, Y.Q.; Wang, P.Y.; Theakstone, W.H.; An, W.L.; Wang, X.F.; Lu, A.G.; Zhang, W.; Cao, W.H. Changes of daily climate extremes in southwestern China during 1961–2008. *Glob. Planet. Chang.* **2011**, *80–81*, 255–272. [[CrossRef](#)]
46. Wang, H. The weakening of the Asian monsoon circulation after the end of the 1970s. *Adv. Atmos. Sci.* **2001**, *18*, 376–386. [[CrossRef](#)]
47. Hung, C.; Kao, P. Weakening of the winter monsoon and abrupt increase of winter rainfalls over northern Taiwan and southern China in the early 1980s. *J. Clim.* **2010**, *23*, 2357–2367. [[CrossRef](#)]
48. Gao, J.Q.; Yang, X.G.; Dong, C.Y.; Li, K.N. Precipitation resource changed characteristics in arid and humid regions in Northern China with climate changes. *Trans. Chin. Soc. Agric. Eng.* **2015**, *31*, 99–110. [[CrossRef](#)]
49. Dong, L.; Zhang, M.J.; Wang, S.J.; Zhu, X.F.; Ren, Z.G.; Wang, Q. Extreme Precipitation Events in Arid Areas in Northwest China Based on Gridded Data. *J. Nat. Resour.* **2014**, *29*, 2048–2057. [[CrossRef](#)]
50. Wang, H.M.; Li, Z.H.; Han, G.D. The analysis on the spatial-temporal change of climate aridity in Xilinguole Steppe. *Acta Ecol. Sin.* **2010**, *30*, 6538–6545.
51. Bao, G.; Liu, Y.; Liu, N.; Linderholm, H.W. Drought variability in eastern Mongolian Plateau and its linkages to the largescale climate forcing. *Clim. Dyn.* **2015**, *44*, 717–733. [[CrossRef](#)]

